

**A genuine correlation in piezoelectric properties of
two-dimensional materials: a high-throughput computational
study**

Cihan Arlı and Tuğbey Kocabaş

*Department of Materials Science and Engineering, Institute of Graduate Program,
Eskisehir Technical University, Eskiehir, TR 26555, Turkey*

Deniz Çakır

*Department of Physics and Astrophysics,
University of North Dakota, Grand Forks,
North Dakota 58202, United States*

Cem Sevik*

*Department of Mechanical Engineering, Faculty of Engineering,
Eskisehir Technical University, Eskiehir, TR 26555, Turkey*

(Dated: February 17, 2020)

Abstract

The rational design of two-dimensional piezoelectric materials has recently garnered increasing interest because of harnessing these materials in technological applications, including sensor technology, actuating devices, energy harvesting, and medical applications. Several materials possessing high piezoelectric response have been reported so far, but a high-throughput first-principles approach to estimate the piezoelectric potential of layered materials has not been performed yet. In this respect, we systematically investigated the piezoelectric (e_{11} , d_{11}) and elastic (C_{11} and C_{12}) properties of 108 thermodynamically stable two-dimensional (2D) semiconductor materials by employing first-principle methods. Our calculations found a notable difference between the relaxed ion coefficients calculated with GGA and LDA functionals, indicating a strong exchange-correlation functional dependence. Nevertheless, both functionals yield the same trends for the elastic constants and piezoelectric coefficients. Our high-throughput approach demonstrates that the materials containing Group-V elements produce notably high piezoelectric strain constants, $d_{11} > 40 \text{ pmV}^{-1}$, and 42 of considered materials have the e_{11} coefficient higher than MoS_2 inasmuch as BrSSb has one of the largest d_{11} with a value of 503.6 pmV^{-1} . Besides, we established simple empirical models to estimate the d_{11} coefficients by utilizing the relative ionic motion in the unit cell and the polarizability of the individual elements in the compounds. The proposed models, tested for both exchange-correlation functionals, are successful in estimating the piezoelectric constants of the studied materials with sufficient accuracy.

I. INTRODUCTION

Piezoelectricity, a phenomenon that occurs in a semiconductor material without inversion-symmetry when it electrically polarizes in response to applied mechanical stress, is of utmost importance for sensing, actuating, and energy harvesting applications. Therefore, it has been attracted notable attention scientifically and technologically for the years. Recently, first-principles calculations on layered materials further have triggered a great interest in this physical property and its applications. The piezoelectric strain coefficients (d_{11}), which is a measure of the mechanical to electrical energy conversion efficiency, of various two-dimensional materials such as single-layer nitrides, gapped graphene, transition metal dichalcogenides (TMDCs), transition metal dioxides (TMDOs), group III and IV monochalcogenides, and II-VI and IIIV compounds, have been determined as one or two orders of magnitude larger than that of traditionally used bulk materials such as α -quartz ($d_{11} = 2.3 \text{ pmV}^{-1}$)^{1,2}, *wurtzite*-GaN ($d_{33} = 3.1 \text{ pmV}^{-1}$)³, and *wurtzite*-AlN ($d_{33} = 5.1 \text{ pmV}^{-1}$)³. Considering various 2D materials, the values as high as 7.39, 8.47, 10.3, 16.3, 21.7, 27.3, 212.1, 250.5 pmV^{-1} have been obtained for monolayers, MoTe₂⁴, CrSe₂⁵, MoSTe⁶, CrTe₂⁵, CdO⁴, SnOSe⁷, GeSe⁸, and SnSe⁸ crystals, respectively. In addition to these theoretical calculations, experimental studies have also demonstrated the intriguing piezoelectric response of 2D materials. Li *et al.* indirectly verified the existence of *h*-BN monolayer piezoelectricity⁹ and Ares *et al.* measured the e_{11} coefficient of this material as $2.91 \times 10^{-10} \text{ Cm}^{-1}$ ¹⁰. Wu *et al.* experimentally affirmed piezoelectricity in free-standing monolayer MoS₂, they found that this material exhibits a strong piezoelectric effect for an odd number of layers in which case inversion symmetry is broken¹¹ and most recently Dai *et al.* demonstrated that the piezoelectric properties of the monolayer MoS₂ can be tailored by addition of grain boundaries¹². Zhu *et al.* measured the e_{11} coefficient of this monolayer material as $2.9 \times 10^{-10} \text{ Cm}^{-1}$, conforming the previous theoretical calculations¹³. Lu *et al.* demonstrated the piezoelectric response in monolayer MoSS¹⁴. Also, Zelisko *et al.* determined the e_{11} for *g*-C₃N₄ as $2.18 \times 10^{-10} \text{ Cm}^{-1}$ ¹⁵.

Indeed, these results have overtly revealed that layered materials possess high piezoelectric as well as flexoelectric responses, which makes them very appealing for the next generation nanoscale technological applications such as stretchable smart electronics, skins, switches and many types of sensors. In fact, when the further enhancement of this excit-

ing property via nanoengineering is considered^{16,17} as previously demonstrated for several physical properties, the importance of this field of research becomes more prominent.

On the other hand, these developments offer vast opportunities for computational material science since a large number of materials can now be searched and classified without experimentation, and simple models can be developed using generated numerous data to estimate promising materials. Practically, the valuable information generated in that sense may potentially pave the way rapid design and development of device applications based on the 2D piezoelectric/flexoelectric materials.

Considering that fact, we performed a high throughput materials search study to predict the promising 2D hexagonal and trigonal crystals with large piezoelectric responses that can be exploited for device applications. We selected thermodynamically stable semiconductor materials without inversion symmetry from the Computational 2D Materials Database (C2DB)¹⁸. Our first-principles calculations and empirical models provided a fundamental understanding of the correlation between piezoelectric properties of 108 monolayers and basic features (atomic mass and polarizability) of the constituent elements. Besides, we found that the relative motion of atoms within monolayer against the external stress determines the size of net polarization and thereby piezoelectric coefficients. As a result, we identified the most promising materials with a large piezoelectric response.

II. COMPUTATIONAL DETAILS

First principle calculations based on density functional theory (DFT) were performed as implemented in the Vienna Ab initio Simulation Package (VASP) code¹⁹⁻²¹. Exchange-correlation effects were included using both local density approximation (LDA) and generalized gradient approximation (GGA) within Perdew-Burke-Ernzerh formalism (PBE)²². Single-electron wave functions were expanded up to an energy-cutoff of 550 eV for the structural relaxations and 700 eV for elastic and piezoelectric constant calculations. Brillouin-zone integrations were performed using a Γ -centered regular $24 \times 24 \times 1$ k -point mesh within the MonkhorstPack²³ scheme. The convergence criteria for the electronic and ionic relaxations were set to 10^{-6} eV and 10^{-5} eV \AA^{-1} (10^{-4} eV \AA^{-1} for LDA calculations), respectively. To prevent artificial interlayer interactions, the vacuum space was taken at least 15 \AA for all considered structures. Piezoelectric coefficient tensor e_{ijk} and elastic stiffness tensor C_{ijkl}

were calculated directly by using density functional perturbation theory (DFPT)²⁴.

A. Theoretical Background

Two different functionals, namely local density approximation (LDA) and Perdew-Burke-Ernzerhof (PBE) form of generalized gradient approximations (GGA), were used to identify the exchange-correlation (XC) functional dependence in our calculations. For solids, it is known that the PBE functional gives under binding, i.e., yielding larger bonding distances as compared to LDA, resulting in smaller elastic constants. As we show later, this also affects the piezoelectric responses of the materials.

The piezoelectric phenomenon is an electromechanical coupling and occurs only in certain non-centrosymmetric semiconducting materials where an electric dipole moment develops upon the application of stress or strain. The coefficients describing piezoelectric effect, namely e_{ijk} and d_{ijk} , are given as

$$e_{ijk} = \frac{\partial \mathbf{P}_i}{\partial \varepsilon_{jk}} = \frac{\partial \sigma_{jk}}{\partial E_i} \quad (1)$$

$$d_{ijk} = \frac{\partial \mathbf{P}_i}{\partial \sigma_{jk}} = \frac{\partial \varepsilon_{jk}}{\partial E_i} \quad (2)$$

$$e_{ik} = d_{ij} C_{jk} \quad (3)$$

where $j, k = 11, 22, 33, 12, 23, 31, i = 1, 2, 3$, \mathbf{P}_i , E_i , ε_{jk} and σ_{jk} are piezoelectric polarization, macroscopic electric field, strain and stress, respectively. In the Voigt notation, e_{ijk} and d_{ijk} are reduced to e_{il} and d_{il} , respectively, where $l \in 1, 2, \dots, 6$.

Based on the symmetry of the crystals, there exist certain amounts of independent elastic and piezoelectric constants. These independent constants depend on the point group symmetry of the crystals. Elastic response (elasticity), which is related to the mechanical properties of a material, can be identified as a reaction of the material on a macroscopic (or microscopic) scale to an external force²⁵. Elasticity is an anisotropic property that is identified with 4th rank tensor and represented with a 6×6 matrix²⁶. On the other hand, the piezoelectric constant is a third rank tensor and represented by a 3×6 matrix in 3-dimensional space.

The 7, 34, 28, 7, and 31 of the 107 materials considered in this study can be classified into six different prototype structures, namely GeSe, MoSSe (also known as Janus system), BiTeI, GaS, and MoS₂, respectively. The crystal structures of these prototypes and test

case h -BN are illustrated in Fig. 1 (a-f). While MoSSe, BiTeI, and GeSe have trigonal $3m$ symmetry, MoS₂, GaS, and h -BN have hexagonal $\bar{6}m2$ symmetry. Note that the hexagonal $\bar{6}m2$ symmetry system is a special type of the trigonal $3m$ system. Hexagonal $\bar{6}m2$ exhibits mirror symmetry in the out of the plane direction, which nullifies the e_{31} , d_{31} , and C_{14} constants. However, MoSSe and BiTeI prototypes include two different cation atoms with different atomic sizes and electronegativities, which gives rise to two inequivalent anion-cation bond lengths and charge distributions. As a result, the reflection symmetry is broken in the out-of-plane direction, resulting in a nonzero dipole moment and e_{31} and d_{31} are reflected in the piezoelectric tensors.

The elastic and piezoelectric strain and stress tensors for trigonal $3m$, and hexagonal $\bar{6}m2$ symmetries can be described respectively as;

$$C_{jk} = \begin{pmatrix} C_{11} & C_{12} & C_{13} & C_{14} & \cdot & \cdot \\ C_{12} & C_{11} & C_{13} & -C_{14} & \cdot & \cdot \\ C_{13} & C_{13} & C_{33} & \cdot & \cdot & \cdot \\ C_{14} & -C_{14} & \cdot & C_{44} & \cdot & \cdot \\ \cdot & \cdot & \cdot & \cdot & C_{44} & C_{14} \\ \cdot & \cdot & \cdot & \cdot & C_{14} & \frac{C_{11}-C_{12}}{2} \end{pmatrix} \quad (4)$$

$$e_{ik} = \begin{pmatrix} e_{11} & -e_{11} & \cdot & \cdot & e_{15} & \cdot \\ \cdot & \cdot & \cdot & e_{15} & \cdot & -e_{11} \\ e_{31} & e_{31} & e_{33} & \cdot & \cdot & \cdot \end{pmatrix} \quad (5)$$

$$d_{ij} = \begin{pmatrix} d_{11} & -d_{11} & \cdot & \cdot & d_{15} & \cdot \\ \cdot & \cdot & \cdot & e_{15} & \cdot & -2d_{11} \\ d_{31} & d_{31} & d_{33} & \cdot & \cdot & \cdot \end{pmatrix} \quad (6)$$

and,

$$C_{jk} = \begin{pmatrix} C_{11} & C_{12} & C_{13} & \cdot & \cdot & \cdot \\ C_{12} & C_{11} & C_{13} & \cdot & \cdot & \cdot \\ C_{13} & C_{13} & C_{33} & \cdot & \cdot & \cdot \\ \cdot & \cdot & \cdot & C_{44} & \cdot & \cdot \\ \cdot & \cdot & \cdot & \cdot & C_{44} & \cdot \\ \cdot & \cdot & \cdot & \cdot & \cdot & \frac{C_{11}-C_{12}}{2} \end{pmatrix} \quad (7)$$

$$e_{ik} = \begin{pmatrix} e_{11} & -e_{11} & \cdot & \cdot & \cdot & \cdot \\ \cdot & \cdot & \cdot & \cdot & \cdot & -e_{11} \\ \cdot & \cdot & \cdot & \cdot & \cdot & \cdot \end{pmatrix} \quad (8)$$

$$d_{ij} = \begin{pmatrix} d_{11} & -d_{11} & \cdot & \cdot & \cdot & \cdot \\ \cdot & \cdot & \cdot & \cdot & \cdot & -2d_{11} \\ \cdot & \cdot & \cdot & \cdot & \cdot & \cdot \end{pmatrix} \quad (9)$$

The algorithms implemented in the VASP code calculate these tensors assuming periodic boundary conditions in 3D. But for 2D materials, stress and strain are constrained in the basal plane, nullifying the stress/strain components for σ_3/ε_3 , σ_4/ε_4 and σ_5/ε_5 . Therefore, one can obtain a 2D representation of the elastic constants and piezoelectric coefficient for matrices trigonal $3m$, and hexagonal $\bar{6}m2$ symmetries respectively as follows:

$$C_{jk} = \begin{pmatrix} C_{11} & C_{12} & \cdot \\ C_{12} & C_{11} & \cdot \\ \cdot & \cdot & \frac{C_{11}-C_{12}}{2} \end{pmatrix} \quad (10)$$

$$e_{ik} = \begin{pmatrix} e_{11} & -e_{11} & \cdot \\ \cdot & \cdot & -e_{11} \\ e_{31} & e_{31} & \cdot \end{pmatrix} \quad (11)$$

$$d_{ij} = \begin{pmatrix} d_{11} & -d_{11} & \cdot \\ \cdot & \cdot & -2d_{11} \\ d_{31} & d_{31} & \cdot \end{pmatrix} \quad (12)$$

and,

$$C_{jk} = \begin{pmatrix} C_{11} & C_{12} & \cdot \\ C_{12} & C_{11} & \cdot \\ \cdot & \cdot & \frac{C_{11}-C_{12}}{2} \end{pmatrix} \quad (13)$$

$$e_{ik} = \begin{pmatrix} e_{11} & -e_{11} & \cdot \\ \cdot & \cdot & -e_{11} \\ \cdot & \cdot & \cdot \end{pmatrix} \quad (14)$$

$$d_{ij} = \begin{pmatrix} d_{11} & -d_{11} & \cdot \\ \cdot & \cdot & -2d_{11} \\ \cdot & \cdot & \cdot \end{pmatrix} \quad (15)$$

where, $i, j, k = 1, 2, 3$. Then from Eq. 15, d_{11} and d_{31} become;

$$d_{11} = \frac{e_{11}}{C_{11} - C_{12}} \quad (16)$$

$$d_{31} = \frac{e_{31}}{C_{11} + C_{12}} \quad (17)$$

d_{31} do not vanishes for monolayers with broken out-of-plane inversion symmetry. From Equations 10-15, one can see that only independent components are e_{11} , d_{11} , e_{31} , d_{31} , and C_{11} , C_{12} for the structures considered in this study.

Since the calculations were performed for 3D cells with vacuum layer in the z -direction, the coefficients were renormalized by multiplying with the z lattice parameter to get 2D constants, *i.e.*, $C_{ij}^{2D} = zC_{ij}^{3D}$ and $e_{ij}^{2D} = ze_{ij}^{3D}$. This rescaling also changes the units of the constants from Nm^{-2} to Nm^{-1} and Cm^{-2} to Cm^{-1} for the C_{ijk} and e_{ik} , respectively. Then the unit for d_{ij} becomes mV^{-1} .

III. RESULTS AND DISCUSSIONS

As mentioned above, we investigated 108 (including h -BN) semiconductor two-dimensional materials without inversion symmetry, found as thermodynamically stable in the Computational 2D Materials Database (See also Table S1-S8 and Figures S1-S2 in the Supporting Information, SI). As expected, the piezoelectric properties of some of the materials considered in our calculations were previously investigated with density functional perturbation theory (DFPT) and/or Berry Phase (BP) approach^{4,27-30}. The satisfactory agreement, depicted in Fig. 2 (See also Table S9 in SI), between our results and the ones published the literature clearly demonstrate the accuracy of the approach used in this work.

Note that, for the materials presented by red dots (GeS, GeSe, SnS, and SnSe), there is a considerable difference between the calculated d_{11} values, and the ones obtained by Hu and Dong²⁷. In fact, the consistency in calculated e_{11} values in these two cases demonstrates that the significant differences arise from the elastic constants, C_{11} and C_{12} obtained in these two cases, yielding different in d_{11} values. Indeed, our elastic constant values are in good agreement with the values presented in C2DB database.

A. Effect of Functional

To shed light on the impact of XC functional on the piezoelectric properties, we considered both LDA and PBE exchange-correlation functionals in the simulations. PBE functional predicts larger interatomic bond distances, which leads to smaller elastic constants values as compared to LDA (See also Figures S1-S52 in SI). These results are also in good agreement with the work done by Råsander and Moram³¹. They also found that the elastic constants, C_{11} , and C_{12} are smaller in the case of PBE functional compared to LDA. The difference between GGA and LDA functionals is about 10% for the materials belonging to the MoSSe, MoS₂, and BiTeI prototypes and 15-20 % for those belongs to the GeSe and GaS prototypes.

When the piezoelectric strain constants, e_{11} , are analyzed, the results exhibit a much-complicated trend. Although the difference between the clamped ion values obtained with both functionals is in a reasonable range (around $\pm 15\%$), there are salient differences between the relaxed ion values. These coefficients naturally include the polarization effects due to the displacement of atoms, which is different for each monolayer. In fact, LDA and PBE capture these displacements and bond strengths distinctively, and thus, the relaxed-ion constants are substantially different for each functional in some cases. For 28 materials, relaxed ion e_{11} coefficients obtained with these two functionals are in reasonable agreement with the difference only around $\pm 10\%$. However, PBE functional yields larger values, on average 20-25% for GeSe, BiTeI and MoSSe, even up to 50% for the GaS prototypes as compared to LDA. LDA functional predicts larger values for some materials classified in the MoSSe and MoS₂ prototypes. Conspicuously, there are some counter materials, namely the ZrSTe, ZrSeTe, HfSeTe, TiSSe, and CaI₂, HfTe₂, ZrTe₂, MgCl₂ belonging to MoSSe and MoS₂ prototypes, which shows a significant difference between PBE and LDA values (100-800%). Six of these materials has Zr or Hf (IVB group) as cation and S, Se and/or Te (VIA group) as the anion. It seems that remarkable differences are limited to certain compositions. When the Zr or Hf cation is bonded with, for example, a VIIA group element, the difference becomes reasonable. To clear out the nature of the effect of functionals on the piezoelectric properties, we also investigated some selected materials such as TiSSe ($e_{11}^{LDA} > e_{11}^{GGA}$) and AsIS ($e_{11}^{GGA} > e_{11}^{LDA}$) via the BP approach (See also Table-S10 in SI). We can state that the source of a remarkable difference in d_{11} coefficients predicted with PBE and LDA is due to the larger ionic displacement in the corresponding direction under the tensile

or compressive strain.

Despite these significant differences between the values calculated with different functionals, it can be said with full confidence that the trends between the piezoelectric properties of the materials studied are independent of the used functional. Accordingly, unless otherwise stated, we present the results obtained by employing PBE functional.

B. Piezoelectric Properties

When prototypes are compared, materials belonging to the MoSSe prototype yield larger piezoelectric constants. The origin of this behavior is attributed to the relative motion of anions in the lattice against applied strain. For this prototype, both anions move in the same direction giving rise to increased polarization, and hence, a larger piezoelectric effect. In sharp contrast, the anions in monolayers with BiTeI type structure move in the opposite directions, resulting in a reduced polarization, thereby smaller piezoelectric constants. The amount of net polarization is sensitive to the atomic polarizability (P) to the mass (M) ratio of constituent atoms (polarizability to mass ratio P/M). This statement is discussed further in the following parts, but briefly, the individual atomic polarization to mass ratio can be used as a good indicator of the piezoelectric response.

The sub-group of MoSSe prototype containing Sb cation yields the highest values, see Table I. Among them, the BrSSb possesses a quite high d_{11} value of 503.62 pmV⁻¹. In prototype BiTeI, the highest values are obtained by the three materials comprising As cation, see Table I. The only difference in the chemical composition of these materials is the anions. Therefore, the difference in piezoelectric coefficients can be explained by the P/M values of I (0.259), Br (0.263), and Cl (0.422). One should note that the AsIS material exhibits the largest piezoelectric coefficient among these three materials, but the element I has the lowest P/M value. This is because the anions in BiTeI prototype move in the opposite directions. PbS₂ structure has the exceptionally high d_{11} value of 91.7 pmV⁻¹ within the MoS₂ prototype in which the average d_{11}^{PBE} value is 3.57 pmV⁻¹ when excluding PbS₂. However, the e_{11} value of PbS₂ is not that high when compared with the other materials in this prototype. The distinctly smaller C_{11} to C_{12} ratio (this is also the case for BrSSb structure in MoSSe prototype) results in an enhanced d_{11} value for this monolayer. The materials classified in GaS prototype give the lowest results with the average d_{11} value of

TABLE I: The relaxed ion e_{11} and d_{11} coefficients for the most promising candidate monolayers.

MoSSe Prototype				
Material	$e_{11}(10^{-10} \text{ Cm}^{-1})$		$d_{11}(\text{pmV}^{-1})$	
	PBE	LDA	PBE	LDA
BrSSb	11.7	8.3	503.6	173.8
ISSb	11.3	8.6	195.6	90.6
BrSbSe	9.8	7.1	141.3	76.5
BiTeI Prototype				
Material	$e_{11}(10^{-10} \text{ Cm}^{-1})$		$d_{11}(\text{pmV}^{-1})$	
	PBE	LDA	PBE	LDA
AsIS	21.2	13.3	95.7	40.9
AsBrS	13.9	9.4	49.4	27.3
AsClS	11.9	7.8	36.6	20.8
MoS2 Prototype				
Material	$e_{11}(10^{-10} \text{ Cm}^{-1})$		$d_{11}(\text{pmV}^{-1})$	
	PBE	LDA	PBE	LDA
PbS ₂	2.4	2.0	91.7	87.3

1.9 pmV⁻¹. Also, the difference between the LDA and PBE calculations is the lowest in this prototype. Consequently, as a result of systematic investigation performed in this study, we predicted 70, 38, 24, and 13 materials possess a piezoelectric strain coefficient greater than 3.64 (that of MoS₂), 10, 20, and 50 pmV⁻¹, respectively.

C. Empirical Model

In literature, there are some empirical models proposed to estimate the d_{11} values of the materials, considering the ratio between the polarizability of the anion to cation. In general, these models do not count the potential ionic motion due to the external effect, which has a notable influence on the final value, according to our analysis discussed below. Blonsky

*et al.*⁴, stated that for the MX₂ materials (where M = Cr, Mo, W, Nb, Ta, and X = S, Se, Te) there is a direct correlation between the polarizability ratio of anion and cation, *i.e.*, P_{anion}/P_{cation} (where P is the polarizability of an atom), and piezoelectric constants of these materials. However, the correlation is valid only when a distinct correlation constant used for each M atom.

In this respect, we developed a different approach, which includes the effect of the polarizability of the atoms and the ionic motion as well. This approach leads to further understanding of why some of the materials possess enhanced piezoelectric properties. Considering the mechanism of the piezoelectricity, which involves polarization of the crystal due to an external effect, four mechanisms emerge; I. The electronic component of polarization, II. Ionic motion, III. Molecular orientation, and IV. Mobile charge carriers under external field³². For the case of piezoelectric response, the electronic components and ionic motion mechanisms are the main mechanisms.

The electronic component of the polarization occurs when the electron cloud around the nucleus changes the orientation in favor of one way. This effect can be observed in all the constituent ions³². Therefore, we consider the atomic polarizability values in the proposed model. For the ionic motion mechanism, the situation is different. The material cannot experience a translation when subjected to deformation, meaning that the center of mass does not change when stress or strain is applied to the crystal, or under a piezoelectric response. Thus, heavier atoms must move shorter relative to the lighter atoms to keep the center of mass unchanged. Since the ionic motion increases the polarization of a crystal, heavier atoms contribute to overall polarization less due to smaller ionic motion and therefore, the atomic mass is also considered. In addition, bond strength also influences the ionic motion and thereby, we utilized the C_{11} values of the materials as well. To this end, considering three metrics, namely (1) Polarizability³³ of the individual atoms (which has an increasing effect), (2) atomic mass, and (3) elastic constant C_{11} of the crystal (which has a reducing impact on the d_{11} values), we proposed a model as follows to estimate d_{11} coefficients.

$$d_{11} = \frac{m \left[\left(\frac{P_c}{M_c} \right) + 0.5 \left(\left(\frac{P_{a_1}}{M_{a_1}} \right) + \left(\frac{P_{a_2}}{M_{a_2}} \right) \right) \right]}{C_{11}} + c \quad (18)$$

Where m and c are the correlation constants. P, M, and C_{11} are polarizability, atomic mass, and elastic constant, respectively. Subscripts c , a_1 , and a_2 represent the cation, first anion,

and second anion, respectively. The terms corresponding to anions are multiplied by 0.5 to average the contribution of anions collapsing on top of each other in the stereographic projection. As seen in Fig. 3, there is a strong correlation between the coefficients calculated with the proposed simple formula and DFPT calculations.

Here, we used different correlation constants (m and c) as listed in SI (Tables S11-S18 in SI) file for different sub-groups due to the influence of other factors such as the number of valance electron of the constituent atoms and electronegativity. However, the results depict that the piezoelectric coefficients of two-dimensional materials, which consist of a specific anion (see Fig. 3a) and cation or containing a specific cation (see Fig. 3b) can be reasonably estimated with this simple formula which combines the atomic polarizability, atomic mass, and C_{11} . In Eq. 18, the summation of the P/M ratios for anions (*i.e.*, $\frac{P_{a1}}{M_{a1}} + \frac{P_{a2}}{M_{a2}}$) implicitly includes the relative motion of anions within the unit cell. This model is valid for a broad range (50 to 500 pmV⁻¹, see also Table S13 in SI) as seen in the Sb case depicted in see Fig. 3b).

We altered the model proposed for MoS₂ and MoSSe prototypes in the case of BiTeI due to the different ionic motion mechanism of this prototype, as depicted in Fig. 4b and c. In BiTeI crystal, anions occupy the different lattice sites on the monolayer plane, and they move in the opposite direction against the external field (*stress/strain*). Here, we do not include the scale factor of 0.5 since anions are not on top of each other anymore, as see in Fig. 1. And we subtract the contribution of the first anion since it moves in the opposite direction with respect to the second anion (the first anion is from VIIA group element (Cl, I, Br) in the correlation equation). By doing this, we can introduce the relative motion of anions into this simple model. Also, we do not use C_{11} value for this model because, considering the three-atom system, the C_{11} value does not represent which anion has a stronger bond with the cation (stronger bond means less ionic motion). Note that this opposite motion of the anions is unique to the monolayers having BiTeI-type structure. Eventually, in that case, the model takes the following form;

$$d_{11} = m \left(\left(\frac{P_c}{M_c} \right) - \left(\frac{P_{a1}}{M_{a1}} \right) + \left(\frac{P_{a2}}{M_{a2}} \right) \right) + c \quad (19)$$

As seen in Fig. 4, the proposed model for this prototype gives the estimated values with reasonable prediction accuracy and is capable of distinguishing different piezoelectric properties of these materials. Using this simple approach, we are able to acquire a fundamental

TABLE II: . Comparison between BrSSb, ISSb and BrSbSe. P, P/M, TC, d_{11}^P and d_{11}^{DFT} are the polarizability, polarizability to mass ratio, Total Contribution (value between the square brackets in equation 18), predicted d_{11} and calculated d_{11} , respectively. For these materials, correlation constants m and c (in appropriate units) are 66054 and -1492, respectively.

Material	Mass	P	C_{11}	P/M	TC	d_{11}^P	d_{11}^{DFT}
	(g/mol)	(au)	(Nm ⁻¹)			(pmV ⁻¹)	(pmV ⁻¹)
BrSSb							
Sb	121.76	43.00	27.10	0.353	0.787	426.4	503.6
Br	79.90	21.00		0.263			
S	32.07	19.40		0.605			
ISSb							
Sb	121.76	43.00	28.78	0.353	0.785	310.3	195.6
I	126.91	32.90		0.259			
S	32.07	19.40		0.605			
BrSbSe							
Sb	121.76	43.00	27.17	0.353	0.668	130.9	141.3
Br	79.90	21.00		0.263			
Se	78.96	28.90		0.366			

insight into why some materials have better piezoelectric responses. For instance, Table II shows the materials, namely BrSSb, ISSb and BrSbSe, belonging to MoSSe prototype. One can see that the total contribution values are similar for the BrSSb and ISSb materials, but the large difference in the piezoelectric coefficient arises from the C_{11} value, which is smaller for the BrSSb. Since there are not enough materials to create a valid data pool for GeSe and GaS prototypes, we could not investigate the piezoelectric properties of these materials with a model.

IV. CONCLUSION

In this work, we report the elastic and piezoelectric properties of 108 thermodynamically stable 2D materials calculated by employing different exchange-correlation functionals. Our systematic analysis clearly shows that more than 50 crystal possesses the d_{11} coefficient value desired for regarding technological applications. Also, notable systems such as BrSSb, ISSb, BrSbSe, AsIS and PbS₂ were determined to have coefficients comparable with the materials currently used in various scientific and technological fields. Here, we also developed simple, yet effective models based on the relative ionic motions and atomic polarizabilities for predicting the d_{11} coefficient of considered crystals. Our models, which gives reasonable agreement with both GGA-PBE and LDA values as depicted in Figure S55-S60 in Supplementary Information, provide an insight into which type of materials can have better piezoelectric coefficients. Furthermore, it frankly explains the nature of the predicted piezoelectric properties. The dynamic and thermodynamic stability of the considered materials is included in the 2D material database that shows the high chance of synthesizability of these types of materials. We believe that the findings of this research can lead to new experimental studies to realize novel piezoelectric materials for various applications.

Acknowledgments

We acknowledge the support from the Eskisehir Technical University (ESTU-BAP 19ADP080). We also acknowledge financial support from ND EPSCoR through NSF grant OIA-1355466. Computational resources were provided by the High Performance and Grid Computing Center (TRGrid e-Infrastructure) of TUBITAK ULAKBIM, the National Center for High Performance Computing (UHeM) of Istanbul Technical University.

* csevik@eskisehir.edu.tr

¹ V. E. Bottom, *Journal of Applied Physics* **41**, 3941 (1970).

² R. Bechmann, *Phys. Rev.* **110**, 1060 (1958).

³ C. M. Lueng, H. L. W. Chan, C. Surya, and C. L. Choy, *Journal of Applied Physics* **88**, 5360 (2000).

- ⁴ M. N. Blonsky, H. L. Zhuang, A. K. Singh, and R. G. Hennig, ACS Nano **9**, 9885 (2015).
- ⁵ M. M. Alyörük, Y. Aierken, D. Çakır, F. M. Peeters, and C. Sevik, The Journal of Physical Chemistry C **119**, 23231 (2015).
- ⁶ M. Yagmurcukardes, C. Sevik, and F. M. Peeters, Phys. Rev. B **100**, 045415 (2019).
- ⁷ X. Zhang, Y. Cui, L. Sun, M. Li, J. Du, and Y. Huang, J. Mater. Chem. C **7**, 13203 (2019).
- ⁸ R. Fei, W. Li, J. Li, and L. Yang, Applied Physics Letters **107**, 173104 (2015).
- ⁹ Y. Li, Y. Rao, K. F. Mak, Y. You, S. Wang, C. R. Dean, and T. F. Heinz, Nano Letters **13**, 3329 (2013).
- ¹⁰ P. Ares, T. Cea, M. Holwill, Y. B. Wang, R. Roldn, F. Guinea, D. V. Andreeva, L. Fumagalli, K. S. Novoselov, and C. R. Woods, Advanced Materials **32**, 1905504 (2019).
- ¹¹ W. Wu, L. Wang, Y. Li, F. Zhang, L. Lin, S. Niu, D. Chenet, X. Zhang, Y. Hao, T. F. Heinz, et al., Nature **514**, 470 (2014).
- ¹² M. Dai, W. Zheng, X. Zhang, S. Wang, J. Lin, K. Li, Y. Hu, E. Sun, J. Zhang, Y. Qiu, et al., Nano Letters (2019).
- ¹³ H. Zhu, Y. Wang, J. Xiao, M. Liu, S. Xiong, Z. J. Wong, Z. Ye, Y. Ye, X. Yin, and X. Zhang, Nature nanotechnology **10**, 151 (2015).
- ¹⁴ A.-Y. Lu, H. Zhu, J. Xiao, C.-P. Chuu, Y. Han, M.-H. Chiu, C.-C. Cheng, C.-W. Yang, K.-H. Wei, Y. Yang, et al., Nature nanotechnology **12**, 744749 (2017).
- ¹⁵ M. Zelisko, Y. Hanlumuayang, S. Yang, Y. Liu, C. Lei, J. Li, P. M. Ajayan, and P. Sharma, Nature communications **5**, 1 (2014).
- ¹⁶ Y. Lu and S. B. Sinnott, ACS Applied Nano Materials **3**, 384 (2020).
- ¹⁷ F. R. Fan, W. Wu, et al., Research **2019**, 7367828 (2019).
- ¹⁸ *Computational 2d materials database (c2db)*, <https://cmr.fysik.dtu.dk/c2db/c2db.html>, URL <https://cmr.fysik.dtu.dk/c2db/c2db.html>.
- ¹⁹ G. Kresse and J. Furthmüller, Phys. Rev. B **54**, 11169 (1996).
- ²⁰ P. E. Blchl, Phys. Rev. B **50**, 17953 (1994).
- ²¹ G. Kresse and D. Joubert, Phys. Rev. B **59**, 1758 (1999).
- ²² J. P. Perdew, K. Burke, and M. Ernzerhof, Phys. Rev. Lett. **77**, 3865 (1996).
- ²³ H. J. Monkhorst and J. D. Pack, Phys. Rev. B **13**, 5188 (1976).
- ²⁴ X. Wu, D. Vanderbilt, and D. R. Hamann, Phys. Rev. B **72**, 035105 (2005).
- ²⁵ R. Yu, J. Zhu, and H. Q. Ye, Computer Physics Communications **181**, 671 (2010).

- ²⁶ J. F. Nye, *Physical properties of crystals: their representation by tensors and matrices* (Clarendon Press, 1957).
- ²⁷ T. Hu and J. Dong, *Phys. Chem. Chem. Phys.* **18**, 32514 (2016).
- ²⁸ L. Dong, J. Lou, and V. B. Shenoy, *ACS Nano* **11**, 8242 (2017).
- ²⁹ Dimple, N. Jena, A. Rawat, R. Ahammed, M. K. Mohanta, and A. De Sarkar, *J. Mater. Chem. A* **6**, 24885 (2018).
- ³⁰ K.-A. N. Duerloo, M. T. Ong, and E. J. Reed, *The Journal of Physical Chemistry Letters* **3**, 2871 (2012).
- ³¹ M. Rsander and M. A. Moram, *The Journal of Chemical Physics* **143**, 144104 (2015).
- ³² R. E. Newnham, *Properties of materials: anisotropy, symmetry, structure* (Oxford University Press, 2015).
- ³³ P. Schwerdtfeger and J. K. Nagle, *Molecular Physics* **117**, 1200 (2019).

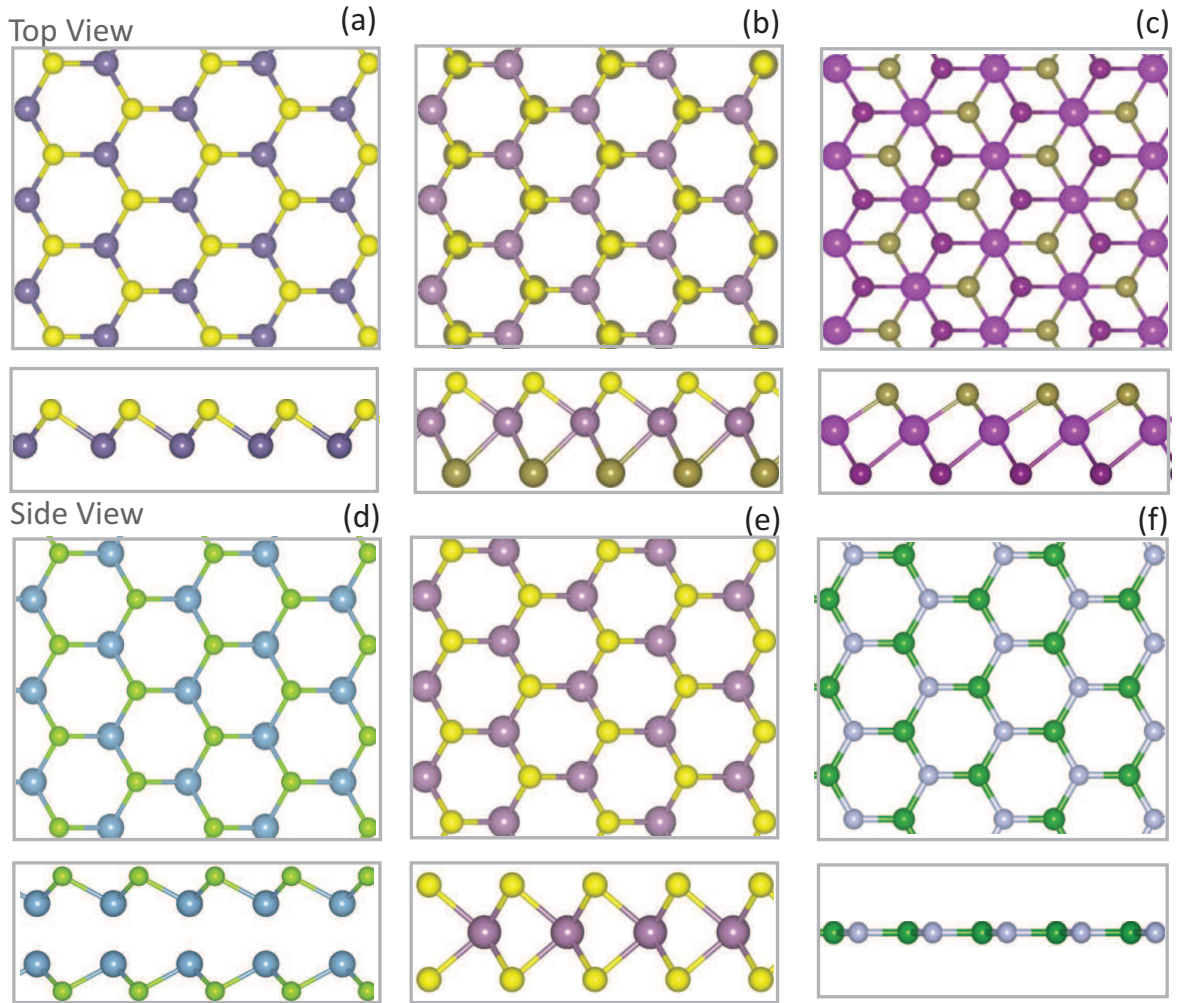


FIG. 1: Top and side views of (a)GeSe, (b)MoSSe, (c)BiTeI, (d)GaS, (e)MoS₂ and (f)h-BN prototypes.

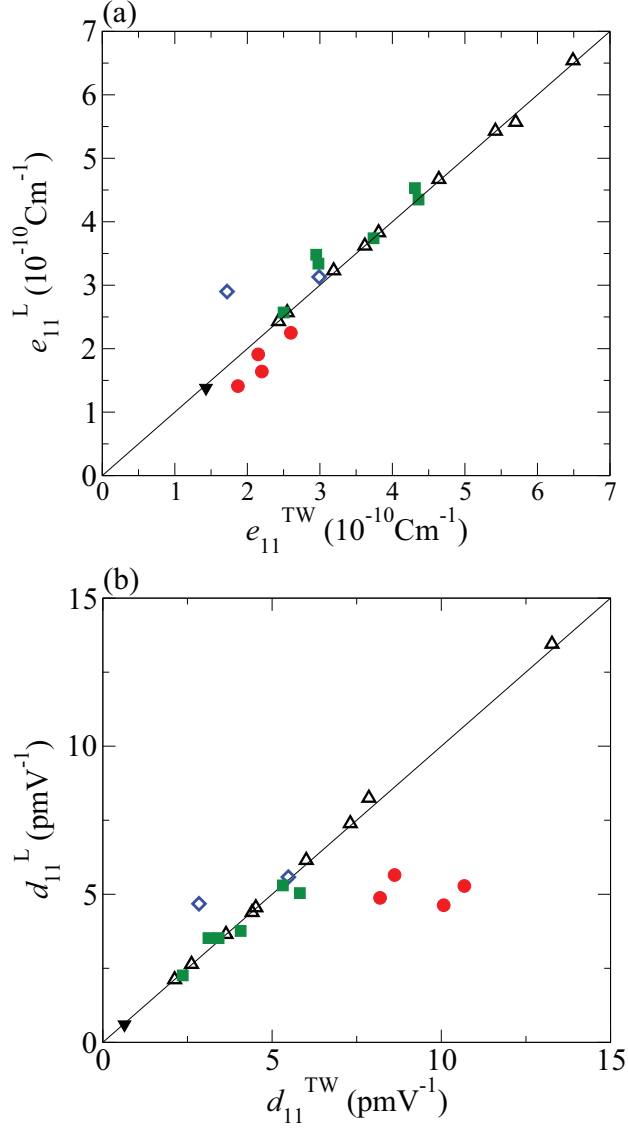


FIG. 2: Comparison of the results calculated in this study and reported in the literature. The filled and unfilled symbols show the literature values obtained by Berry phase (BP) and density functional perturbation theory (DFPT) calculations, respectively. Superscripts L and TW represents literature and this-work. MX_2 (where $M = \text{Cr, M, W}$ and $X = \text{S, Se, Te}$), MSSe (where $M = \text{Hf, Zr}$), MXY (where $M = \text{Mo, W}$ and $X, Y = \text{S, Se, Te}$), MX (where $M = \text{Ge, Sn}$ and $X = \text{S, Se}$) and $h\text{-BN}$ represented by empty black triangle, empty blue diamond, solid green square, solid red dots and solid black triangle, respectively.

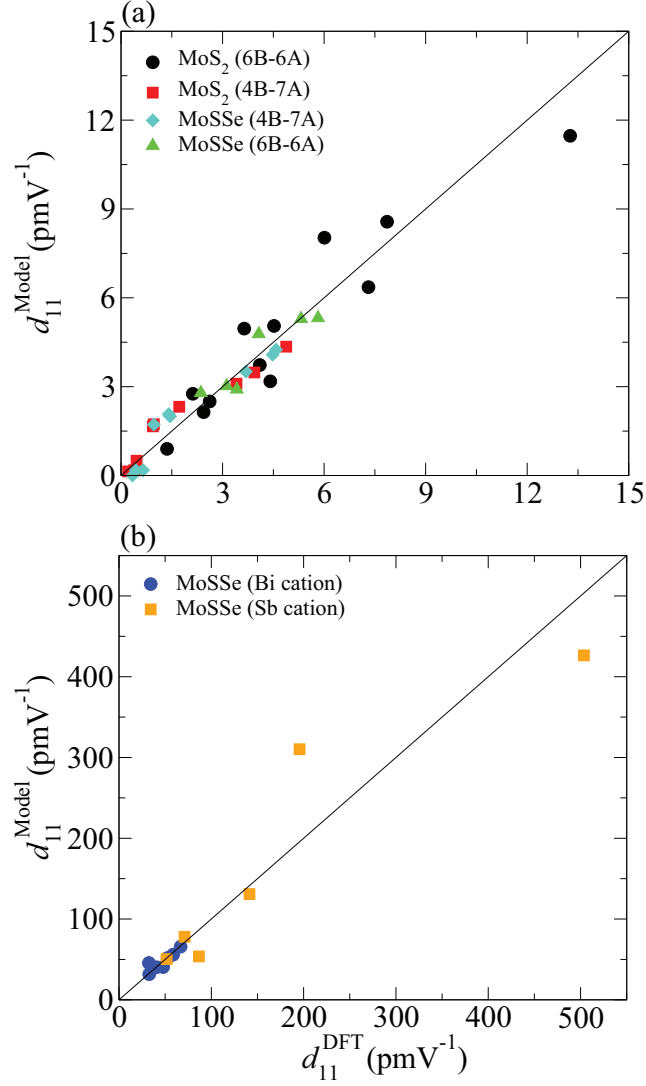


FIG. 3: DFPT and Model comparison for d_{11} of the materials belonging to MoS₂ and MoSse prototypes. (a) Sub-group of MoS₂ prototype containing VIB cation and VIA anion (black circle), sub-group of MoS₂ prototype containing IVB cation and VIIA anion (red square), sub-group of MoSse prototype containing IVB cation and VIIA anion (turquoise diamond), and sub-group of MoSse prototype containing VIB cation and VIA anion (green triangle). (b) Sub-group of MoSse prototype containing Bi cation (blue circle), and sub-group of MoSse prototype containing Sb cation (orange squares).

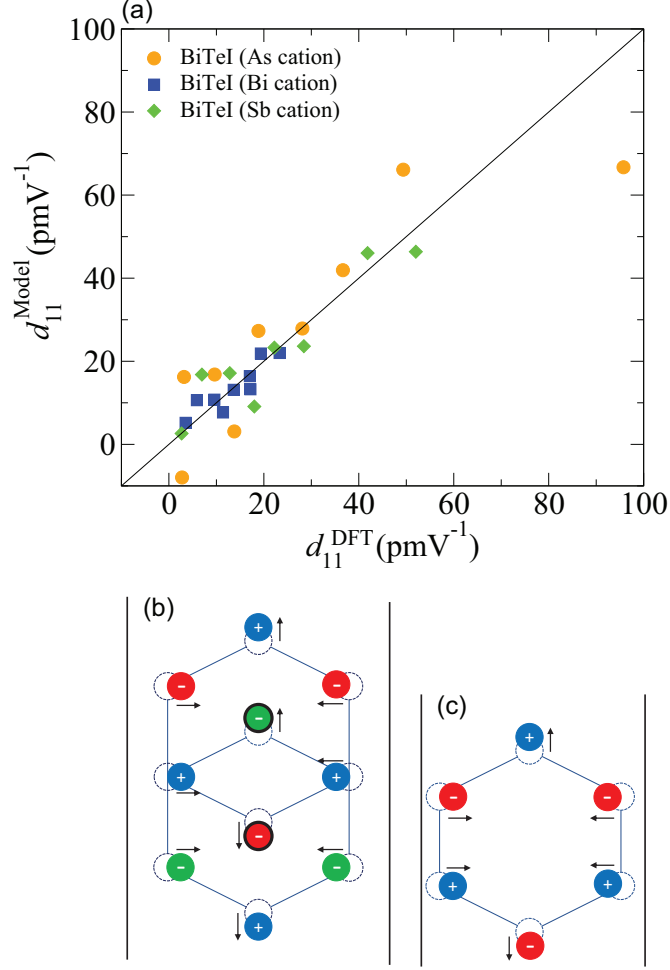


FIG. 4: (a) Comparison of the calculated and predicted d_{11}^{DFT} pmV^{-1} values by using Eq. 19. Orange circles represent the sub-group of BiTeI prototype containing As cation, blue squares represent the sub-group of BiTeI prototype containing Bi cation, green diamonds represent the sub-group of BiTeI prototype containing Sb cation. (b) and (c) Schematically representation of ions for BiTeI and the other prototypes, respectively. Here, atoms represented with solid black circles correspond to the opposite movement.